

Observation of exceptional points in anisotropic ReS_2 microcavities

Huihua Chen(陈辉华), Yuquan Zhou(周玉全), Xin Li(李昕), Jinyang Lou(娄金阳), Song Luo(罗松), Hang Zhou(周航), Xinyue Zhang(张新悦), Zhao Xu(徐钊), Yan Liu(刘艳), Zheng Lv(吕峥), Yuxin Duan(段雨欣), Haodong Cheng(成浩东), Hongming Zhang(张鸿铭), Yaofeng Zhu(朱耀峰), Anpeng Li(李安鹏), Jian Ren(任坚), Xiao Wang(王潇), Lixin Zhang(章立心), Long Zhang(张龙), and Zhanghai Chen(陈张海)
Citation: Chin. Phys. B, 2026, 35 (**5**): 057105. DOI: 10.1088/1674-1056/ae48c8
http://cpb.iphy.ac.cn; http://iopscience.iop.org/cpb

What follows is a list of articles you may be interested in

PT phase transition and non-Hermitian skin effect in vacancy-induced subbands of the Haldane model with gain and loss

Cui-Xian Guo(郭翠仙), Xiao-Ming Zhao(赵小明), and Su-Peng Kou(寇谡鹏)
Chin. Phys. B, 2026, 35 (**4**): 047103. DOI: 10.1088/1674-1056/ae44f4

A two-stage injection locking amplifier based on a cavity magnonic oscillator

Mun Kim, Chunlei Zhang, Chenyang Lu, Jacob Burgess, and Can-Ming Hu
Chin. Phys. B, 2025, 34 (**6**): 067104. DOI: 10.1088/1674-1056/add1bf

Actively tuning anisotropic light—matter interaction in biaxial hyperbolic material α-MoO_3 using phase change material VO_2 and graphene

Kun Zhou(周昆), Yang Hu(胡杨), Biyuan Wu(吴必园), Xiaoxing Zhong(仲晓星), and Xiaohu Wu(吴小虎)
Chin. Phys. B, 2024, 33 (**4**): 047103. DOI: 10.1088/1674-1056/ad23d2

Exciton-polaritons in a 2D hybrid organic-inorganic perovskite microcavity with the presence of optical Stark effect

Kenneth Coker, Chuyuan Zheng(郑楚媛), Joseph Roger Arhin, Kwame Opuni-Boachie Obour Agyekum, and Weili Zhang(张伟利)
Chin. Phys. B, 2024, 33 (**3**): 037102. DOI: 10.1088/1674-1056/ad1484

Non-Hermitian Kitaev chain with complex periodic and quasiperiodic potentials

Xiang-Ping Jiang(蒋相平), Yi Qiao(乔艺), and Junpeng Cao(曹俊鹏)
Chin. Phys. B, 2021, 30 (**7**): 077101. DOI: 10.1088/1674-1056/abfa08

SPECIAL TOPIC — Exciton Physics: Fundamentals, materials and devices

Observation of exceptional points in anisotropic ReS_2 microcavities

Huihua Chen(陈辉华)[†], Yuquan Zhou(周玉全)[†], Xin Li(李昕), Jinyang Lou(娄金阳), Song Luo(罗松), Hang Zhou(周航), Xinyue Zhang(张新悦), Zhao Xu(徐钊), Yan Liu(刘艳), Zheng Lv(吕峥), Yuxin Duan(段雨欣), Haodong Cheng(成浩东), Hongming Zhang(张鸿铭), Yaofeng Zhu(朱耀峰), Anpeng Li(李安鹏), Jian Ren(任坚), Xiao Wang(王潇), Lixin Zhang(章立心), Long Zhang(张龙)[‡], and Zhanghai Chen(陈张海)[§]

Department of Physics, College of Physical Science and Technology, Xiamen University, Xiamen 361005, *China*

(Received 17 January 2026; revised manuscript received 19 February 2026; accepted manuscript online 23 February 2026)

Exceptional points (EPs) are spectral singularities in non-Hermitian systems where eigenvalues and eigenvectors simultaneously coalesce. Manipulating EPs in solid-state systems typically requires complex architectures. Here, based on a hybrid system consisted of few-layer rhenium disulfide (ReS_2) deposited on a distributed Bragg mirror, we demonstrate an all-optical method to dynamically control EPs by harnessing the intrinsic optical anisotropy of ReS_2. By utilizing the incident polarization angle as a dynamic control parameter, we continuously modulate the exciton–photon coupling strength, driving the system from the strong coupling regime to the weak coupling regime. The EPs are manifested as simultaneous coalescence of the real (energy) and imaginary (linewidth) parts of the complex eigenvalues. This dual-degeneracy provides unambiguous experimental evidence for EP formation and the associated collapse of the Hilbert space dimensionality. Our findings establish anisotropic light–matter coupled systems as a robust paradigm for exploring non-Hermitian topology in photonics, enabling polarization-driven topological devices without intricate nanofabrication.

Keywords: exciton-polariton, non-Hermitian physics, exceptional points, optical anisotropy

PACS: 71.36.+c, 03.65.Vf, 78.67.–n, 42.25.Ja

DOI: 10.1088/1674-1056/ae48c8 **CSTR:** 32038.14.CPB.ae48c8

1. Introduction

Exciton-polaritons, arising from the strong coupling between cavity photons and excitons, are intrinsically dissipative light-matter hybrids that have long served as a versatile platform for exploring nonequilibrium quantum phenomena.[1–4] Combining the strong nonlinearity of excitons with the high coherence of photons, these composite bosons have paved the way for macroscopic quantum phenomena such as Bose–Einstein condensation (BEC) and superfluidity.[5–12] Recent advances have further expanded this field into two-dimensional transition metal dichalcogenides (TMDs) and perovskites, achieving room-temperature operation and novel device functionalities.[13–20] Furthermore, the enduring vitality of this platform is evidenced by continuous breakthroughs, where recent studies have extended polariton condensation to novel material systems through mechanisms such as bound states in the continuum and quantum dot confinement.[21–23]

In particular, exciton-polariton systems are intrinsically dissipative, which provide a solid-state platform for exploring non-Hermitian physics and topology at the nanoscale.[24–27] Central to this domain are exceptional points (EPs), spectral singularities where the effective non-Hermitian Hamiltonian exhibits the coalescence of not only its eigenvalues but also its eigenvectors.[28–31] Unlike trivial degeneracies in Hermitian systems, EPs correspond to critical branch points on the complex Riemann surface.[32,33] This unique spectral structure has fueled a surge of research into exotic phenomena. For instance, recent works have explored EP-induced knot structures in non-Abelian braids[33] and the steering of entanglement in cavity magnomechanics,[34] alongside established applications in symmetry-breaking-induced sensing[35,36] and chiral mode switching.[37]

Despite their theoretical allure, experimentally accessing and actively manipulating these singularities in solid-state devices remains a significant challenge. Current strategies often rely on breaking parity-time (PT) symmetry through precise gain-loss engineering or fabricating complex nanostructures to induce asymmetric scattering.[26,38,39] Furthermore, navigating the system to an EP requires a versatile mechanism to continuously tune the coherent and dissipative interactions, a capability that is often lacking in static structures.[40] As demonstrated in previous studies,[41–43] the topology of exciton-polariton systems is dictated by the interplay between the coherent coupling rate and the dissipation difference. An exceptional point arises specifically when the coherent interaction exactly compensates for the loss mismatch. This condition manifests experimentally as the simultaneous collapse of

[†]These authors contributed equally to this work.

[‡]Corresponding author. E-mail: zhanglong@xmu.edu.cn

[§]Corresponding author. E-mail: zhanghai@xmu.edu.cn

© 2026 Chinese Physical Society and IOP Publishing Ltd. All rights, including for text and data mining, AI training, and similar technologies, are reserved.

the energy levels and linewidths into a single degenerate state, providing unambiguous evidence of the non-Hermitian phase transition.[41–43]

To realize such precise control without complex lithography, naturally anisotropic van der Waals materials have emerged as a promising alternative.[44] In particular, rhenium disulfide (ReS_2) stands out due to its distorted 1T structure (triclinic symmetry), which features Peierls-distorted rhenium chains.[45] This low-symmetry crystal structure dictates that the excitonic dipoles are strictly linearly polarized and pinned to the crystal axis. Recent engineering of twisted ReS_2 homojunctions has further confirmed the robustness of this polarization anisotropy for enhanced visual intelligence,[46] validating its potential as a stable control knob.[47–50] While Rydberg states and basic polariton formations have been observed in ReS_2,[51–53] and theoretical works have proposed non-Hermitian features in anisotropic materials,[54] a simplified, active strategy to continuously drive the system to the EP singularity using polarization tuning remains to be fully experimentally established.

Here, we experimentally demonstrate the realization and deterministic search for EPs by integrating anisotropic ReS_2 into a planar distributed Bragg reflector (DBR) architecture. In this system, the dispersive Bragg modes hybridize with ReS_2 excitons, where the coupling strength is dictated by the geometric projection of the electric field onto the transition dipoles. By simultaneously scanning the incidence angle and the polarization angle, we map the system's trajectory across a two-dimensional parameter space, which allows for the precise and convenient identification of EPs. This active manipulation drives the system from the strong coupling regime to the weak coupling regime. Crucially, at the transition boundary, we identify the simultaneous crossing of the energy levels and linewidths, providing unambiguous evidence of EP traversal. Our findings establish natural material anisotropy as a straightforward, lithography-free paradigm for navigating non-Hermitian parameter spaces in solid-state photonics.

2. Intrinsic optical anisotropy and self-hybridized modes of ReS_2

Unlike hexagonal TMDs, ReS_2 crystallizes in a low-symmetry triclinic structure, resulting in significant intrinsic in-plane optical anisotropy.[41,44] This symmetry reduction dictates that the excitonic states are strictly linearly polarized and pinned to specific crystallographic directions. Specifically, the two fundamental exciton species, X_1 and X_2, exhibit distinct dipole orientations: the X_1 dipole aligns parallel to the crystallographic b-axis, while the X_2 dipole is oriented at approximately 75° relative to the b-axis.[41,43] Consequently, the light-matter interaction strength is no longer a scalar invariant but follows a projection law $g \propto |\boldsymbol{E} \cdot \boldsymbol{d}|$, where $\boldsymbol{E}$ is the cavity photon polarization and $\boldsymbol{d}$ is the excitonic dipole vector. This intrinsic linear dichroism provides the physical basis for continuous tuning of the coupling strength via polarization rotation, distinguishing ReS_2 as a unique platform for anisotropic photonics.

To characterize the polarization dependence of the excitonic response in ReS_2, we performed polarization-resolved spectroscopy on a mechanically exfoliated crystal transferred onto a 100 nm gold reflector, as schematically illustrated in Fig. 1(a). The resulting experimental polarization-resolved reflectance spectra, presented in Fig. 1(b), reveal a rich manifold of resonance peaks dominated by two fundamental excitonic transitions, denoted as X_1 ($\sim$ 1.55 eV) and X_2 ($\sim$ 1.57 eV). To characterize their in-plane anisotropy, the corresponding angle-resolved absorption polar plots are explicitly presented in Supplementary Fig. S1. These peaks originate from the direct transitions between the conduction band minimum and the two highest valence bands split by crystal field and spin–orbit coupling.[41,44] Close inspection reveals that each exciton peak is further split into two distinct branches rather than appearing as a single resonance. This splitting arises because the thick ReS_2 flake acts as a natural Fabry–Pérot microcavity due to its high refractive index; the confined optical modes within the flake strongly couple with the excitons, leading to the formation of self-hybridized exciton-polaritons, as elucidated in previous studies.[48] Furthermore, prominent reflectance features observed in the higher energy region ($\sim$ 1.65 eV) are attributed to the excited Rydberg states,[46] confirming the robust excitonic binding energy and high crystalline quality of our sample. The numerical simulation results are presented in Fig. 1(c), which exhibit excellent agreement with the experimental data by successfully reproducing the key polarization-dependent features. This includes the angular evolution of the exciton modes and the characteristic splitting associated with self-hybridization. It is worth noting that the Rydberg states observed in the experiment are absent in the simulation, as the theoretical dielectric function included only the fundamental exciton oscillators. These results collectively demonstrate that the coupling strength in the ReS_2 system is intrinsically linked to the light polarization, setting the stage for the active navigation of non-Hermitian singularities discussed in the subsequent sections.

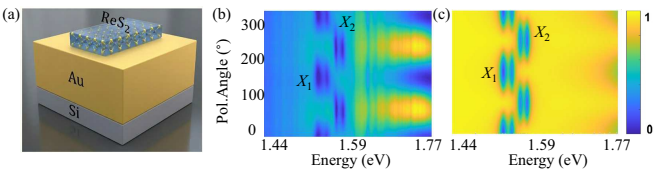


Fig. 1. Optical anisotropy of ReS_2. (a) Schematic of the device: a few-layer ReS_2 deposited on a gold reflector. (b) Polarization-resolved reflectance spectra. Features include X_1 ($\sim$ 1.55 eV) and X_2 ($\sim$ 1.57 eV) exciton branches, their polaritonic doublet splitting, and higher-energy Rydberg states ($\sim$ 1.65 eV). (c) Simulation corresponding to (b).

3. Navigation of exceptional points via polarization control

To investigate the non-Hermitian topology, we constructed a planar microcavity by integrating a mechanically exfoliated ReS_2 flake onto a SiO_2/TiO_2 DBR. In this architecture, the steeply dispersive Bragg modes of the DBR provide a highly confined optical field that strongly hybridizes with the excitons in the ReS_2 layer. Although ReS_2 hosts multiple excitonic resonances, the energy separation between them allows us to treat the system as an effective two-level system within the spectral window of interest. Specifically, due to the large detuning of the secondary exciton relative to the cavity mode near the EP, its contribution is perturbative. Thus, the system dynamics are accurately captured by a 2×2 Hamiltonian involving only the cavity photon and the dominant excitonic mode. The dynamics of this coupled exciton-polariton system are governed by an effective non-Hermitian Hamiltonian, which can be expressed in the basis of the cavity photon (ψ_C) and the exciton (ψ_X) as

$$\boldsymbol{H}_{\text{eff}} = \begin{pmatrix} \omega_C - \mathrm{i}\gamma_C & g \\ g & \omega_X - \mathrm{i}\gamma_X \end{pmatrix}, \tag{1}$$

where $\omega_{C(X)}$ and $\gamma_{C(X)}$ denote the resonance frequency and damping rate (half-linewidth) of the Bragg mode and the exciton, respectively, and g represents the coherent coupling strength. The eigenvalues of this system are given by the complex energies $\lambda_\pm = \bar{\omega} - \mathrm{i}\bar{\gamma} \pm \sqrt{g^2 + \frac{1}{4}(\Delta\omega - \mathrm{i}\Delta\gamma)^2}$, where $\Delta\omega$ is the detuning and $\Delta\gamma$ is the dissipation mismatch. The defining feature of an EP is the simultaneous coalescence of eigenvalues and eigenvectors. While experimental measurements typically access only the spectral information (eigenvalues), the topological nature of the EP can be rigorously inferred from the analytical structure of H_{eff}. In our 2×2 system, at zero detuning ($\Delta\omega = 0$), the square-root discriminant governing the complex eigenvalues simplifies to $\sqrt{g^2 - \Delta\gamma^2/4}$. The EP condition is met strictly when the coupling strength exactly compensates for the dissipation difference ($g = \Delta\gamma/2$), causing the discriminant to vanish. Crucially, for a non-diagonal 2×2 Hamiltonian, the vanishing of this discriminant ensures that the matrix becomes mathematically defective (non-diagonalizable). This implies that the geometric multiplicity of the eigenvalue becomes unity, necessitating the coalescence of the eigenvectors into a single chiral state. Consequently, the simultaneous degeneracy of the real part (energy crossing) and the imaginary part (linewidth crossing) of the eigenvalues serves as a sufficient and robust fingerprint to confirm the formation of an EP and the associated collapse of the Hilbert space dimension.

To experimentally locate the Exceptional Points, we developed a search strategy exploiting the giant optical anisotropy of ReS_2. As established, the effective light-matter coupling strength g in this system is not constant but highly sensitive to the polarization angle ϕ relative to the excitonic dipole. This dependence allows us to continuously tune $g(\phi)$ across the critical threshold defined by the intrinsic dissipation mismatch ($\Delta\gamma/2$). Consequently, by scanning ϕ while

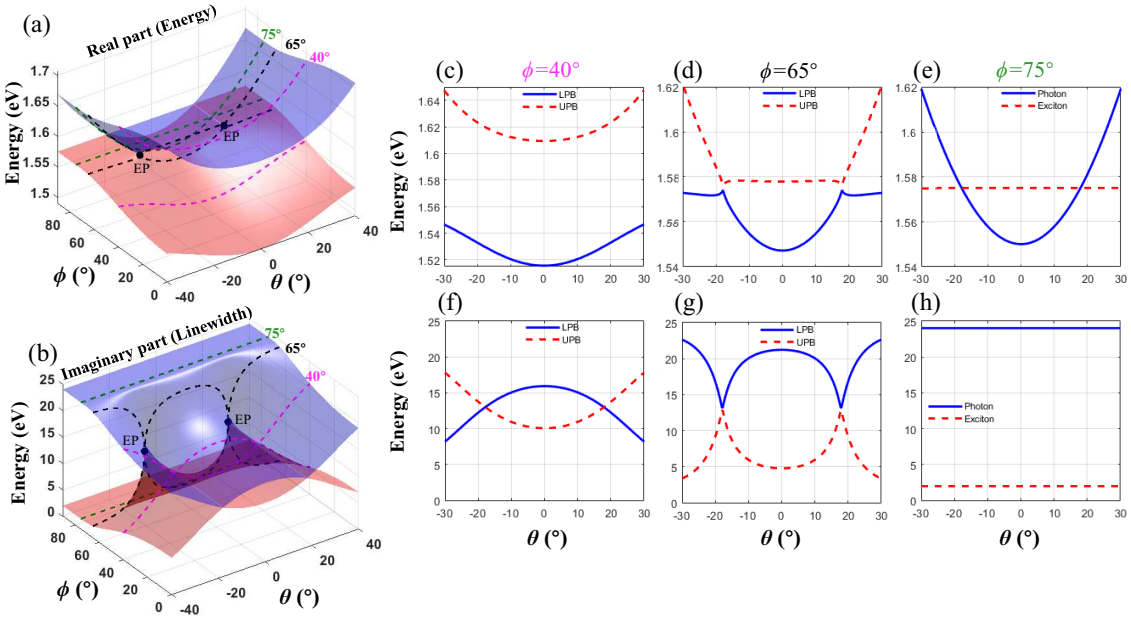


Fig. 2. Navigation of the non-Hermitian topological landscape. (a) and (b) Calculated 3D Riemann surfaces representing the real (energy, (a)) and imaginary (linewidth, (b)) parts of the complex eigenvalues in the two-dimensional parameter space spanned by the incidence angle θ and polarization angle ϕ. The EP marks the singular branch points where the Riemann sheets coalesce. (c)–(h) Evolution of the complex eigenvalue landscape demonstrating the deterministic traversal of the EP. The panels display the energy dispersions (c)–(e) and linewidths (f)–(h) at representative polarization angles: the strong coupling regime ($\phi = 40°$), the critical EP singularity ($\phi = 65°$), and the weak coupling regime ($\phi = 75°$). Note that the EP is identified by the simultaneous degeneracy of both real and imaginary eigenvalues in (d) and (g), distinct from Hermitian degeneracies.

simultaneously varying the exciton–photon detuning Δ (via the incidence angle θ), we can map the system's trajectory through the non-Hermitian parameter space and pinpoint the singularity where $g(\phi) = \Delta\gamma/2$. As illustrated in Figs. 2(c)–2(h), continuously tuning the polarization angle drives the system through a non-Hermitian phase transition, evolving from typical energy anti-crossing (Rabi splitting) in the strong coupling regime ($\phi = 40°$) to linewidth bifurcation in the weak coupling regime ($\phi = 75°$). Crucially, at the transition boundary ($\phi \approx 65°$), we identify a unique spectral degeneracy characterized by the simultaneous coalescence of both the real and imaginary components of the complex eigenvalues (i.e., $\mathrm{Re}(\lambda_+) = \mathrm{Re}(\lambda_-)$ and $\mathrm{Im}(\lambda_+) = \mathrm{Im}(\lambda_-)$). This strict mathematical condition provides unambiguous evidence that the system has successfully traversed the exceptional point.

4. Experimental observation of exceptional points via polarization control

With the specific aim of isolating the EP, we restricted our angle-resolved reflection measurements to transverse electric (TE) polarized light, thereby eliminating the interference from geometric TE–TM splitting. By continuously rotating the incident polarization angle ϕ, we continuously modulated the effective coupling strength $g(\phi)$, thereby driving the system across distinct topological regimes. Figure 3 compares the experimental spectra (Figs. 3(a)–3(c)) with transfer-matrix simulations (Figs. 3(d)–3(f)). At $\phi = 40°$, the system resides in the strong coupling regime (Figs. 3(a) and 3(d)). The spectra exhibit a clear avoided crossing with a robust vacuum Rabi splitting, indicating the formation of well-separated upper and lower polariton branches. As the polarization is rotated to $\phi = 65°$, the system reaches a critical transition point (Figs. 3(b) and 3(e)). Here, the Rabi splitting collapses, and the branches approach a coalesced state near zero detuning. This behavior marks the transition into the EP state, occurring specifically when the coherent coupling rate balances the dissipation difference. Upon further increasing ϕ to 75°, the topology inverts into the weak coupling regime (Figs. 3(c) and 3(f)). The photon dispersion cuts directly through the exciton line without opening a spectral gap, signifying the decoupling of light and matter states. The excellent agreement between experiment and simulation confirms that the coupling regime can be continuously tuned from strong hybridization to the uncoupled state solely via polarization control.

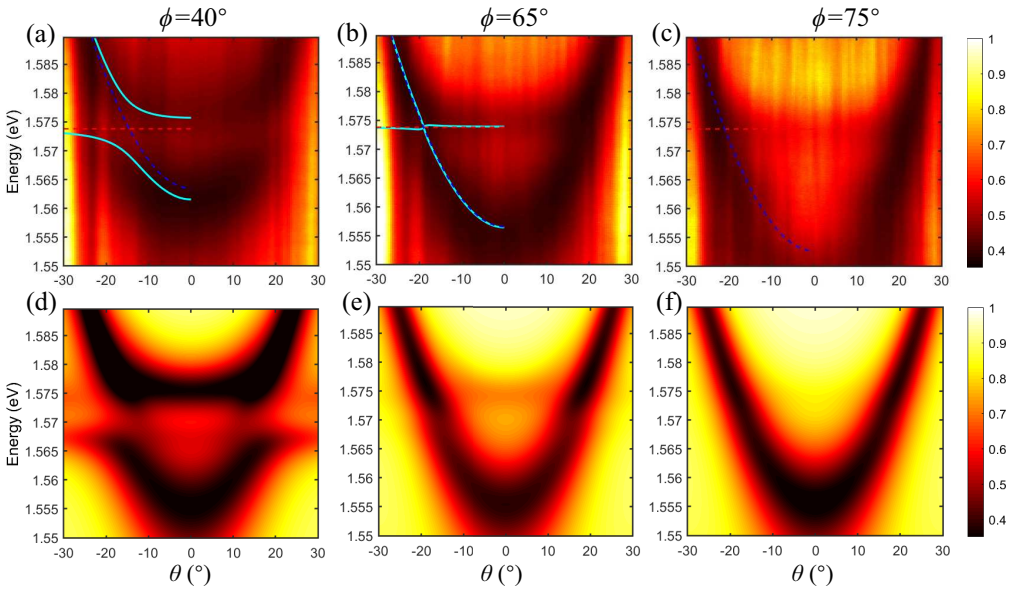


Fig. 3. Experimental identification of the exceptional points. (a)–(c) Experimental angle-resolved reflectance spectra measured at (a) $\phi = 40°$ (strong coupling regime), (b) $\phi = 65°$ (EP regime), and (c) $\phi = 75°$ (weak coupling regime). (d)–(f) Corresponding simulations for the three polarization angles. The evolution from spectral anti-crossing to coalescence and finally to level crossing is clearly reproduced.

To move beyond the qualitative observation of spectral evolution and precisely characterize the EP, we performed a quantitative analysis of the system's complex eigenvalues. Specifically, the energy positions (real part) and linewidths (imaginary part) of the hybrid modes were extracted from the experimental angle-resolved reflection spectra using a dual-peak Lorentzian fitting model with a linear background (see supplementary Fig. S3). Figure 4 displays the angular dependence of these parameters for three representative polarization configurations, serving as a rigorous map to pinpoint the non-Hermitian singularity.

We first analyze the strong coupling regime at $\phi = 40°$ (Figs. 4(a) and 4(d)). The real part of the eigenvalues exhibits a distinct Rabi splitting of approximately 18 meV at zero detuning ($\theta \approx 0°$), indicative of coherent energy exchange. In contrast, the imaginary parts (linewidths) in Fig. 4(d) inter-

sect and cross each other. This combination — energy anti-crossing accompanied by linewidth crossing — is the standard signature of the strong coupling regime where the coupling strength g exceeds the dissipation difference. The scenario is strikingly inverted in the weak coupling regime at $\phi = 75°$ (Figs. 4(c) and 4(f)). Here, the real parts of the eigenvalues become nearly degenerate at zero detuning, showing a crossing trend without a resolvable gap opening. Simultaneously, the imaginary parts undergo a dramatic bifurcation (Fig. 4(f)), splitting into a narrow exciton-like branch and a broad photon-like branch. This significant linewidth contrast confirms that the system is overdamped, with the coupling rate insufficient to synchronize the decay of the two modes.

As predicted by our effective Hamiltonian, the EP occurs strictly when the square-root discriminant vanishes — a state achieved here as the polarization-tuned coupling $g(\phi)$ exactly balances the dissipation mismatch $\Delta\gamma/2$. Mathematically, the EP is a singular spectral degeneracy with zero volume. However, due to finite mode broadening and experimental resolution, this singularity manifests as a finite "EP region" ($\phi \approx 63°$–$67°$). We identify $\phi \approx 65°$ as the optimal EP condition exhibiting the most complete spectral degeneracy, with detailed analysis provided in supplementary Fig. S4. In the energy dispersion (Fig. 4(b)), the upper and lower branches exhibit a "quasi-coalescence" behavior. Although a minute residual splitting remains due to experimental resolution limits, the energy difference is minimized to the noise floor, and the dispersion curves merge tangentially near $\theta = 24°$, consistent with the topological coalescence characteristic of the EP. Crucially, this energy behavior is accompanied by a concomitant evolution in the imaginary domain (Fig. 4(e)). At the same critical angle ($\theta \approx 24°$) where energy splitting is minimized, the linewidths of the two modes also maximally approach each other without crossing. While a perfect intersection is strictly limited by the spectral resolution and sample inhomogeneity, this simultaneous proximity to degeneracy in both real and imaginary parts ($\lambda_+ = \lambda_-$) is the hallmark of non-Hermitian topology. As established in our theoretical derivation, since g remains finite, this eigenvalue coalescence necessitates that the Hamiltonian becomes mathematically defective. This ensures the collapse of eigenvectors into a single chiral state and a corresponding reduction in Hilbert space dimensionality. Unlike Hermitian degeneracies where only one component merges, this simultaneous approach to degeneracy in both real and imaginary parts definitively proves the system has reached the non-Hermitian singularity.

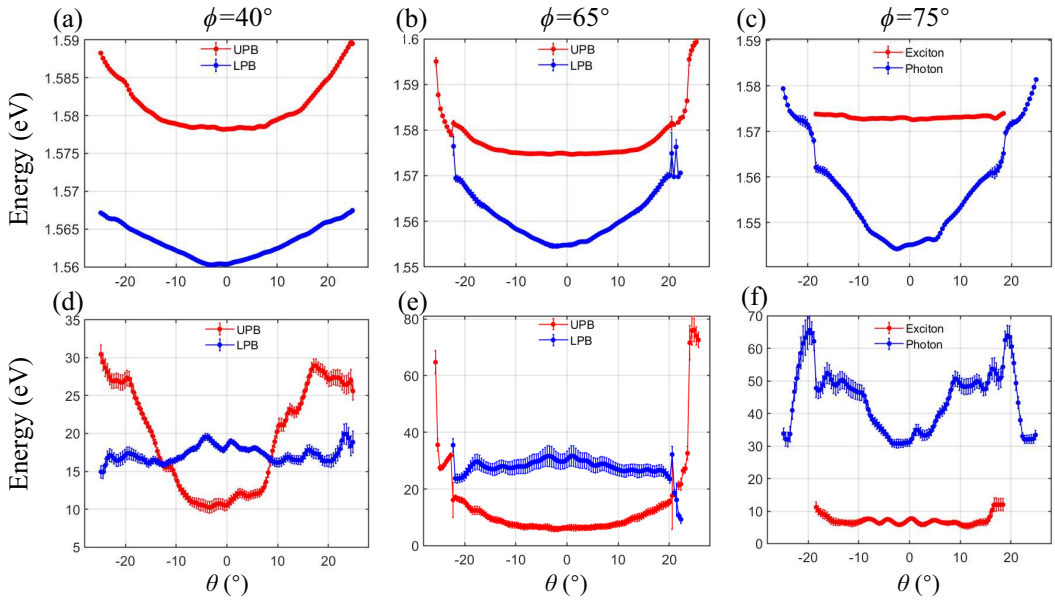


Fig. 4. Quantitative evidence of the exceptional points. (a)–(f) Evolution of real (a)–(c) and imaginary (d)–(f) eigenvalues. (a) and (d) Strong coupling ($\phi = 40°$) features energy anti-crossing and linewidth crossing. (c) and (f) Weak coupling ($\phi = 75°$) displays the inverted behavior: energy crossing and linewidth bifurcation. (b) and (e) At $\phi = 65°$, the simultaneous proximity to degeneracy in both energy and linewidths identifies the EP vicinity. Despite a minute residual splitting from resolution limits, the eigenvalue evolution confirms the non-Hermitian singularity and dimensionality collapse.

5. Conclusion and perspectives

In summary, we have experimentally identified exceptional points by harnessing the intrinsic optical anisotropy of ReS_2 integrated onto a planar DBR architecture. Our work established a lithography-free non-Hermitian platform where light-matter interactions are intrinsically governed by the polarization of incident light. This capability enables continuous navigation of the system trajectory through the non-Hermitian parameter space, driving a smooth topological transition from the strong coupling regime, characterized by Rabi splitting, to the weak coupling regime marked by level crossing. Crucially, quantitative analysis confirms the simultaneous coalescence of

energy levels and linewidths at the transition boundary. This observed dual-degeneracy provides rigorous experimental evidence for the formation of EP and the associated collapse of the Hilbert space dimensionality. Our findings establish natural material anisotropy as a robust paradigm for exploring non-Hermitian topology in exciton-polariton systems. This polarization-tunable architecture opens versatile avenues for next-generation devices, including ultra-sensitive topological sensors, polarization-gated optical switches, and chiral mode converters, all achieved without the need for intricate spatial patterning.

Acknowledgments

Project supported by the National Key R&D Program of China (Grant Nos. 2022YFA1206700, 2023YFA1407100, 2022YFA1204700, and 2023ZD0300300) and the National Natural Science Foundation of China (Grant Nos. W2541001, 12574079, 12304347, 12504373, 62175207, and 92250301).

References

[1] Weisbuch C, Nishioka M, Ishikawa A and Arakawa Y 1992 *Phys. Rev. Lett.* **69** 3314
[2] Sanvitto D and Kéna-Cohen S 2016 *Nat. Mater.* **15** 1061
[3] Luo S, Zhou H, Zhang L and Chen Z 2023 *Appl. Phys. Rev.* **10** 011316
[4] Zhang L and Chen Z 2021 *Sci. Sin. Phys. Mech. Astron.* **51** 030003
[5] Kasprzak J, Richard M, Kundermann S, Baas A, Jeambrun P, Keeling J M J, Marchetti F M, Szymańska M H, André R, Staehli J L, Savona V, Littlewood P B, Deveaud B and Dang L S 2006 *Nature* **443** 409
[6] Deng H, Haug H and Yamamoto Y 2010 *Rev. Mod. Phys.* **82** 1489
[7] Carusotto I and Ciuti C 2013 *Rev. Mod. Phys.* **85** 299
[8] Plumhof J D, Stöferle T, Mai L, Scherf U and Mahrt R F 2014 *Nat. Mater.* **13** 247
[9] Byrnes T, Kim N Y and Yamamoto Y 2014 *Nat. Phys.* **10** 803
[10] Ballarini D, De Giorgi M, Cancellieri E, Houdré R, Giacobino E, Cingolani R, Bramati A, Gigli G and Sanvitto D 2013 *Nat. Commun.* **4** 1778
[11] Zhu L, Pan Y, Chen L, Wang Z, Zhang F, Yang G, Huang C, Hu W, Zhang L, Zhang Y, Dong H and Zhou W 2023 *Nano Lett.* **23** 7797
[12] Zhao H, Guan Z, Li Q, Chen S, Liu Q, Shao Z K, Zhang Y, Zhu X X, Liu J F, Li B B, Li H, Wang S, Gong Q, Gao Y and Liu W 2025 *Nat. Phys.* **21** 1806
[13] Su R, Ghosh S, Wang J, Liu S, Diederichs C, Liew T C H and Xiong Q 2020 *Nat. Phys.* **16** 301
[14] Liu X, Galfsky T, Sun Z, Xia F, Lin E, Lee Y H, Kéna-Cohen S and Menon V M 2015 *Nat. Photonics* **9** 30
[15] Schneider C, Glazov M M, Korn T, Höfling S and Urbaszek B 2018 *Nat. Commun.* **9** 2695
[16] Gu J, Chakraborty B, Khatoniar M and Menon V M 2019 *Nat. Nanotechnol.* **14** 1024
[17] Zhang L, Gogna R, Burg W, Tutuc E and Deng H 2018 *Nat. Commun.* **9** 713
[18] Koshelev K, Lepeshov S, Liu M, Bogdanov A and Kivshar Y 2018 *Phys. Rev. Lett.* **121** 193903
[19] Huang L, Ge C, Xu B, Wang Y, Li S, Luo X, Zhao H, Zhang D, Zeng Z, Tong Q, Li D, Zhu X, Braun K, Gao T, Wang X and Pan A 2025 *Phys. Rev. Lett.* **135** 096902
[20] Yang C, Huang L, Li Y, Zhai X, Ai Q, Xing C, Yang X, Gu Y and Li P 2025 *Chin. Phys. B* **34** 097803
[21] Wu X, Zhang S, Song J, Deng X, Du W, Zeng X, Zhang Y, Zhang Z, Chen Y, Wang Y, Jiang C, Zhong Y, Wu B, Zhu Z, Liang Y, Zhang Q, Xiong Q and Liu X 2024 *Nat. Commun.* **15** 3345
[22] Georgakilas I, Tiede D, Urbonas D, Mirek R, Bujalance C, Calió L, Oddi V, Tao R, Dirin D N, Rainò G, Boehme S C, Galisteo-López J F, Mahrt R F, Kovalenko M V, Miguez H and Stöferle T 2025 *Nat. Commun.* **16** 5228
[23] Zhu T, Chen Z, Wang X, Huang Z, Zhao H and Wang J 2025 *Chin. Phys. B* **34** 094202
[24] Li X, Wang H, Zhou Y, Luo S, Zhou H, Zhu Y, Zhang H, Zhang L and Chen Z 2024 *Phys. Rev. Mater.* **8** L101002
[25] Miri M A and Alù A 2019 *Science* **363** eaar7709
[26] Özdemir Ş K, Rotter S, Nori F and Yang L 2019 *Nat. Mater.* **18** 783
[27] Li A, Wei H, Cotrufo M, Chen W, Mann S, Ni X, Xu B, Chen J, Wang J, Fan S, Qiu C W, Alù A and Chen L 2023 *Nat. Nanotechnol.* **18** 706
[28] Heiss W D 2012 *J. Phys. A: Math. Theor.* **45** 444016
[29] Berry M V 2004 *Czech. J. Phys.* **54** 1039
[30] Luo X, Cai Y, Yue X, Lin W, Zhu J, Zhang Y and Li F 2023 *Photonics Res.* **11** 610
[31] Dembowski C, Gräf H D, Harney H L, Heine A, Heiss W D, Rehfeld H and Richter A 2001 *Phys. Rev. Lett.* **86** 787
[32] Bergholtz E J, Budich J C and Kunst F K 2021 *Rev. Mod. Phys.* **93** 015005
[33] Bao L, Ning J, Shi A, Peng P, Wang Z, Peng C, Wen S and Liu J 2025 *Chin. Phys. B* **34** 097201
[34] Yu C, Liu W M and Yasir K A 2025 *npj Quantum Mater.* **10** 108
[35] Wiersig J 2014 *Phys. Rev. Lett.* **112** 203901
[36] Park J H, Ndao A, Cai W, Hsu L, Kodigala A, Lepetit T, Lo Y H and Kanté B 2020 *Nat. Phys.* **16** 462
[37] Doppler J, Mailybaev A A, Böhm J, Kuhl U, Girschik A, Libisch F, Milburn T J, Rabl P, Moiseyev N and Rotter S 2016 *Nature* **537** 76
[38] Hodaei H, Hassan A U, Wittek S, Garcia-Gracia H, El-Ganainy R, Christodoulides D N and Khajavikhan M 2017 *Nature* **548** 187
[39] Gao T, Estrecho E, Bliokh K Y, Liew T C H, Fraser M D, Brodbeck S, Kamp M, Schneider C, Höfling S, Yamamoto Y, Nori F, Kivshar Y S, Truscott A G, Dall R G and Ostrovskaya E A 2015 *Nature* **526** 554
[40] Lu Y W 2025 *Phys. Rev. A* **112** 063715
[41] Gao W, Li X, Bamba M and Kono J 2018 *Nat. Photonics* **12** 362
[42] Zhang Y, Zhang Z, Yang Z, Wei X and Liang B 2024 *Chin. Phys. B* **33** 060308
[43] Zhang S, He T and Jin L 2024 *Chin. Phys. Lett.* **41** 027201
[44] Zhou Y, Guo Z, Tarazaga Martín-Luengo A, Lanza C, Álvarez-Pérez G, Yu C, Li C, Xia W, Álvarez Cuervo J, Duan X, Wang Y, Martín-Sánchez J, Nikitin A Y, Yao Y, Li J, Alonso-Gonzalez P and Duan J 2026 *Nat. Nanotechnol.* **21** 23
[45] Aslan B, Chenet D A, Van Der Zande A M, Hone J C and Heinz T F 2016 *ACS Photonics* **3** 96
[46] Wu H, Lin Z, Tan C, Hu G, Luo S and Wang Z 2025 *Adv. Funct. Mater.* **35** 24301
[47] Ho C H and Liu Z Z 2019 *Nano Energy* **56** 641
[48] Echeverry J P and Gerber I C 2018 *Phys. Rev. B* **97** 075123
[49] Arora A, Noky J, Drüppel M, Jariwala B, Deilmann T, Schneider R, Schmidt R, Del Pozo-Zamudio O, Stiehm T, Bhattacharya A, Krüger P, Michaelis De Vasconcellos S, Rohlfing M and Bratschitsch R 2017 *Nano Lett.* **17** 3202
[50] Jadczak J, Kutrowska-Girzycka J, Smoleński T, Kossacki P, Huang Y S and Bryja L 2019 *Sci. Rep.* **9** 1578
[51] Coriolano A, Polimeno L, Pugliese M, Cannavale A, Trypogeorgos D, Di Renzo A, Ardizzone V, Rizzo A, Ballarini D, Gigli G, Maiorano V, Rosyadi A S, Chuang C A, Ho C H, De Marco L, Sanvitto D and De Giorgi M 2022 *Sci. Adv.* **8** eadd8857
[52] Gogna R, Zhang L and Deng H 2020 *ACS Photonics* **7** 3328
[53] Kwon S, Yun T K, Ma P J and Nam S 2025 *Nanophotonics* **14** 1553
[54] Chakrabarty D, Dhara A, Das P, Ghosh K, Chaudhuri A R and Dhara S 2026 *Nano Lett.* **12** 4089